Electronic Supporting Information

Surface reactions of ammonia on ruthenium nanoparticles revealed by ^{15}N and ^{13}C solid-state NMR

Niels Rothermel[1], Hans-Heinrich Limbach[2], Iker del Rosal[3], Romuald Poteau*[3], Gabriel Mencia[3], Bruno Chaudret[3], Gerd Buntkowsky*[1], Torsten Gutmann*[1]

[1] *Technical University of Darmstadt, Institute of Inorganic and Physical Chemistry, Alarich-Weiss-Straße 8, D-64287 Darmstadt, Germany*

[2] *Free Universität of Berlin, Institute of Chemistry and Biochemistry, Takustraße 3, D-14195 Berlin, Germany*

[3] *LPCNO; Université de Toulouse, INSA-CNRS-UPS, Institut National des Sciences Appliquées, 135, Avenue de Rangueil, 31077 Toulouse, France.*

Corresponding authors: gutmann@chemie.tu-darmstadt.de

gerd.buntkowsky@chemie.tu-darmstadt.de

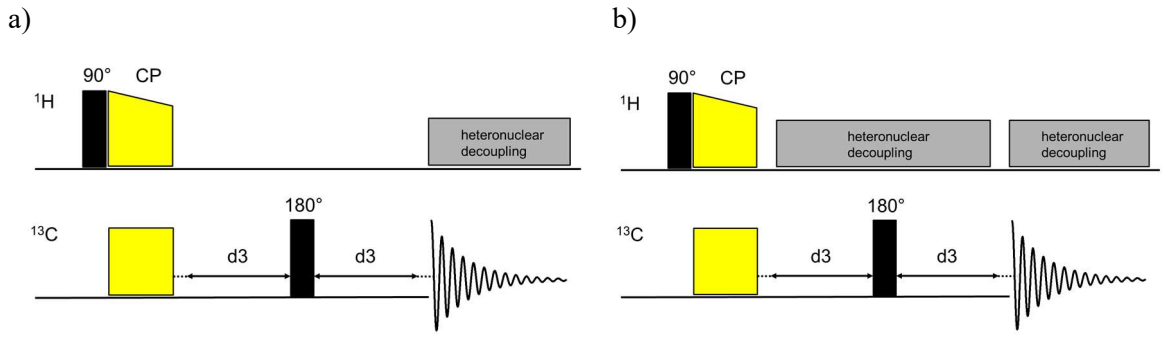

Figure S1. (a) Pulse sequence for the NQS experiment. The dephasing occurs due to the evolution of the spin system under the influence of heteronuclear dipolar coupling during the period d3. (b) Pulse sequence to obtain the reference for the NQS experiment. Here, during the evolution period d3 heteronuclear decoupling is applied. Sequence (a) is implemented in the Topspin 3.2 software package. Sequence (b) was derived from sequence (a).

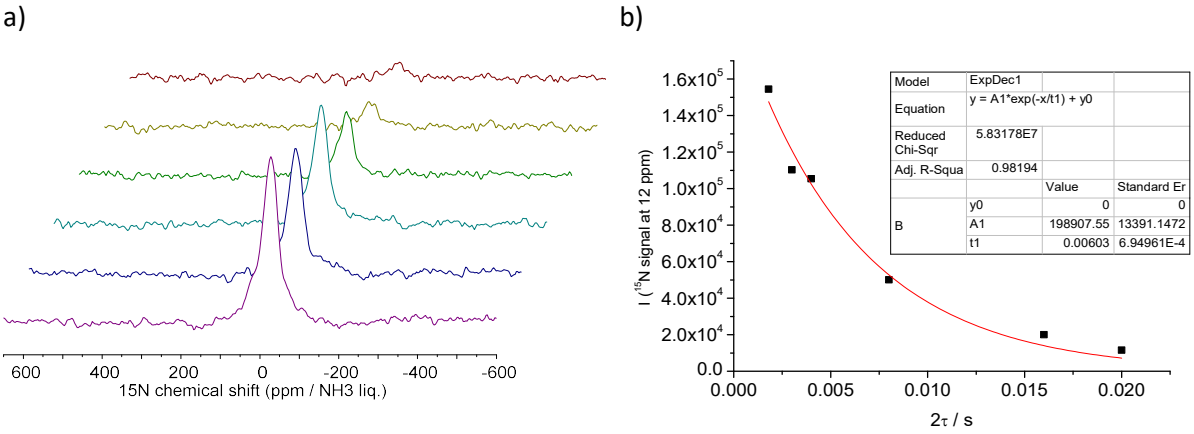

Figure S2. (a) ^{15}N CP MAS echo spectra of the $^{15}NH_3$ treated Ru/dppb sample recorded for different echo spacings τ. (b) Fitting of the analyzed data with an exponential function to obtain the T_2 time (parameter t1 in the fitting).

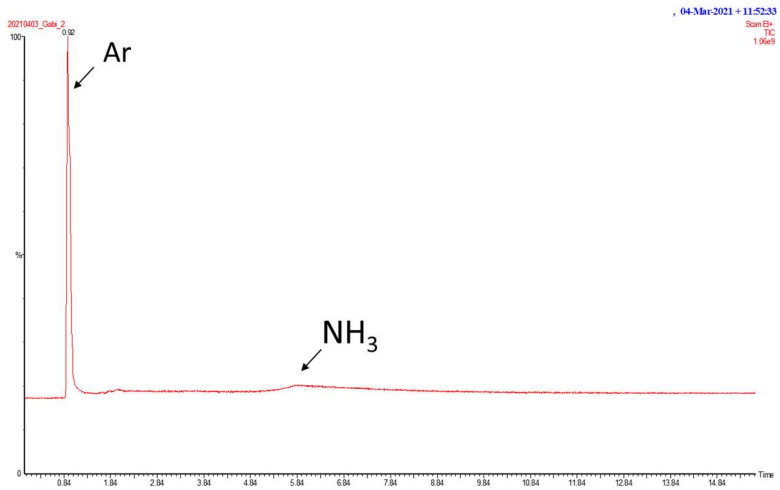

Figure S3. Chromatogram of the gas phase obtained after applying a vacuum to sample **a** and treatment of argon followed by heating at 120°C. Note: The Fischer-Porter bottle was connected directly to the GC-MS system to analyze the composition of the gas phase. A GC-MS method designed for the decomposition of ammonia was employed.

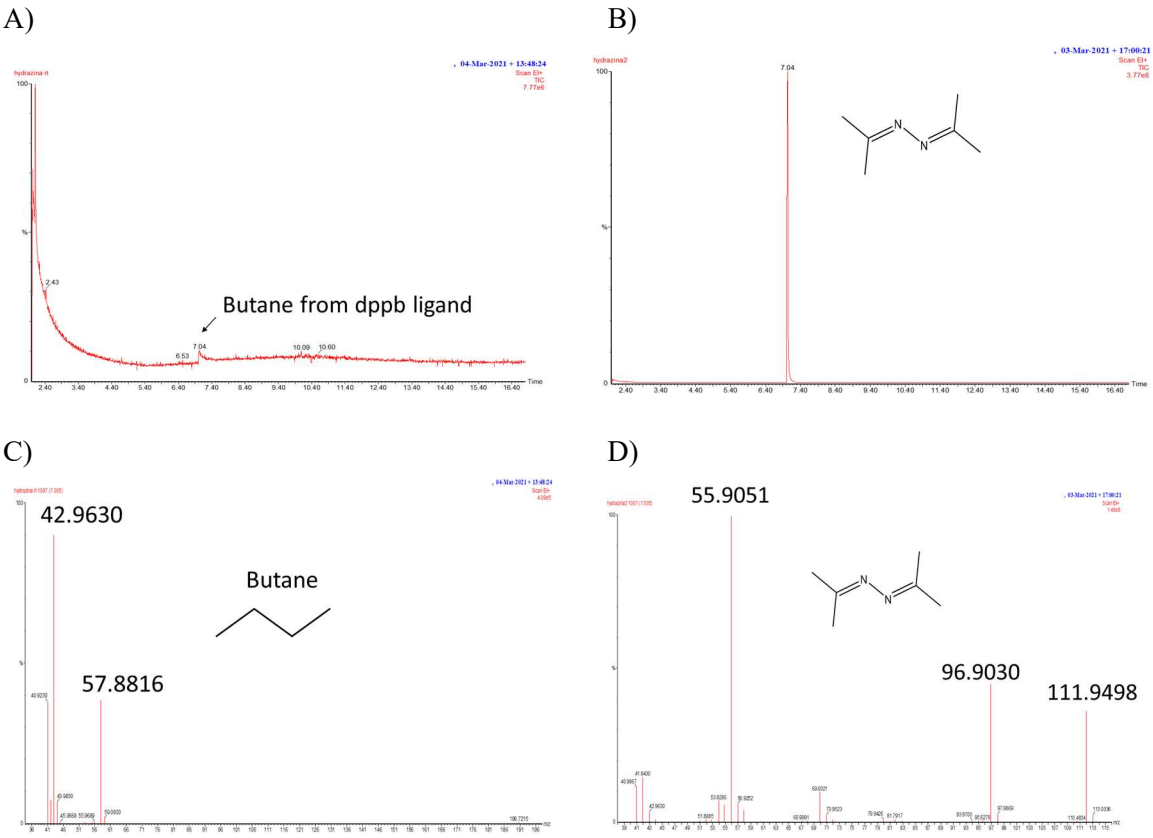

Figure S4. A) Chromatogram of the acetone washing solution obtained from sample **a** at room temperature. B) MS spectrum obtained for the signal at 7.04 min in the chromatogram of the acetone washing solution obtained from sample **a** at room temperature. C) Reference chromatogram of bis-hydrazone. D) Reference MS spectrum of bis-hydrazone. Note: Acetone can react in-situ with hydrazine to form the correspondent bis-hydrazone which can be observed in solution easier than hydrazine. This bis-hydrazone has the same retention time (7.04 min) compared to butane but can be clearly distinguished via the MS analysis.

a)

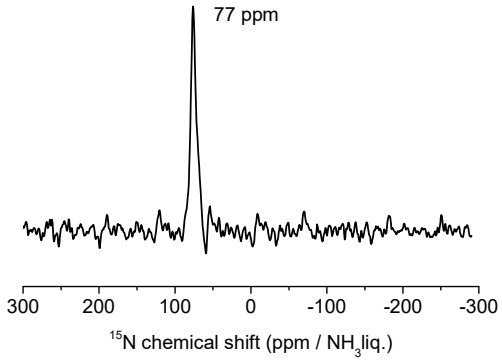

b)

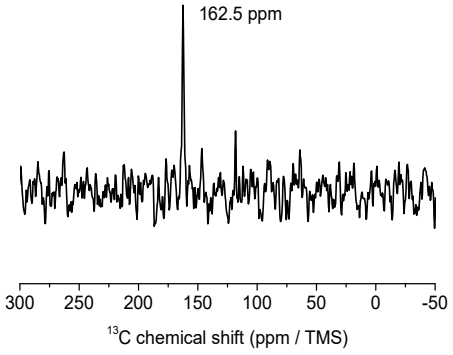

Figure S5. (a) ^{15}N CP MAS spectrum of neat ^{15}N labelled urea measured at 9.4 T and 5 kHz spinning recorded with 128 scans and a repetition delay of 4 s. (b) ^{13}C CP MAS spectrum of ^{15}N labelled urea measured at 9.4 T and 5 kHz spinning recorded with 1 scan. Note: Due to the very long T_1 of protons at room temperature for ^{1}H in urea (app. 1 h) the spectra could only be recorded with moderate S/N.

	ε_d (Ru_s)	ε_d (Ru_c)	q(NH_x)	q(Ru_s)	q(Ru)	q(H)
Ru_{55}	2.57	3.65	-	0.04	0.00	-
$Ru_{55}(NH_3)_{22}$	2.65	3.53	0.09	-0.02	-0.03	-
$Ru_{55}(NH_2)_{22}$	2.83	3.48	-0.33	0.19	0.13	-
$Ru_{55}H_{22}(NH_3)_{22}$	2.74	3.46	0.15	0.10	0.06	-0.27
$Ru_{55}H_{43}(NH_2)_{22}$	3.05	3.26	-0.26	0.36	0.27	-0.21

Table S1. d-band center values (ε_d, in eV) for the 44 surface (Ru_s) and 11 core (Ru_c) Ruthenium atoms in various compounds; q = average Mulliken atomic charges per atom (in |e|, Ru_s atoms, all Ru atoms, NH_x* and H*).

It is noteworthy that the overall charge is positive for NH_3 and negative for NH_2, whereas the metal surface is almost neutral when stabilized by NH_3 only and oxidized when stabilized by NH_2. The surface is of course even more oxidized when hydrides are also present at the surface. The H and NH_2 co-adsorption also significantly stabilizes the surface *d*-band center.

Compound	Energy / eV	μ / μ_B
H2	*-6,770*	
NH3	*-19,543*	
Ru55	*-424,375*	**4,0**
Ru55H22	*-512,813*	**2,0**
Ru55H44	*-598,353*	**2,0**
Ru55H70	*-697,712*	**4,0**
Ru55bare-22topNH3	*-872,427*	**0,0**
Ru55H22-22topNH3	*-957,964*	**0,0**
Ru55bare-22muNH2	*-799,200*	**0,0**
Ru55bare-22mu3NH	*-714,467*	**0,0**
Ru55bare-22muN	*-624,644*	**1,9**
Ru55bare-22mu3N	*-625,545*	**2,0**
Ru55H22-22mu3NH	*-797,511*	**2,0**
Ru55H22-22muNH2	*-883,049*	**0,0**
Ru55H44-22topNH3	*-1042,034*	**0,0**
Ru55H44-22muNH2	*-964,316*	**2,0**
Ru55H55-11topNH3-11muNH2	*-1043,661*	**0,5**
Ru55H44-11topNH3-11muNH2	*-1004,518*	**1,0**
Ru55H33-11topNH3-11muNH2	*-962,978*	**2,0**
Ru55H70-22topNH3	*-1138,974*	**0,0**
Ru55H70-11topNH3-11muNH2	*-1096,599*	**1,0**
Ru55H70-11topNH3-11topNH2	*-1096,038*	**1,0**
Ru55H70-16topNH3-6muNH2	*-1117,634*	**0,0**
Ru55H70-topH10	*-733,327*	**2,0**

Table S2. DFT energies and total electron magnetic moments (μ) of the Ru_{55} NPs model systems and adsorbates considered in this work.

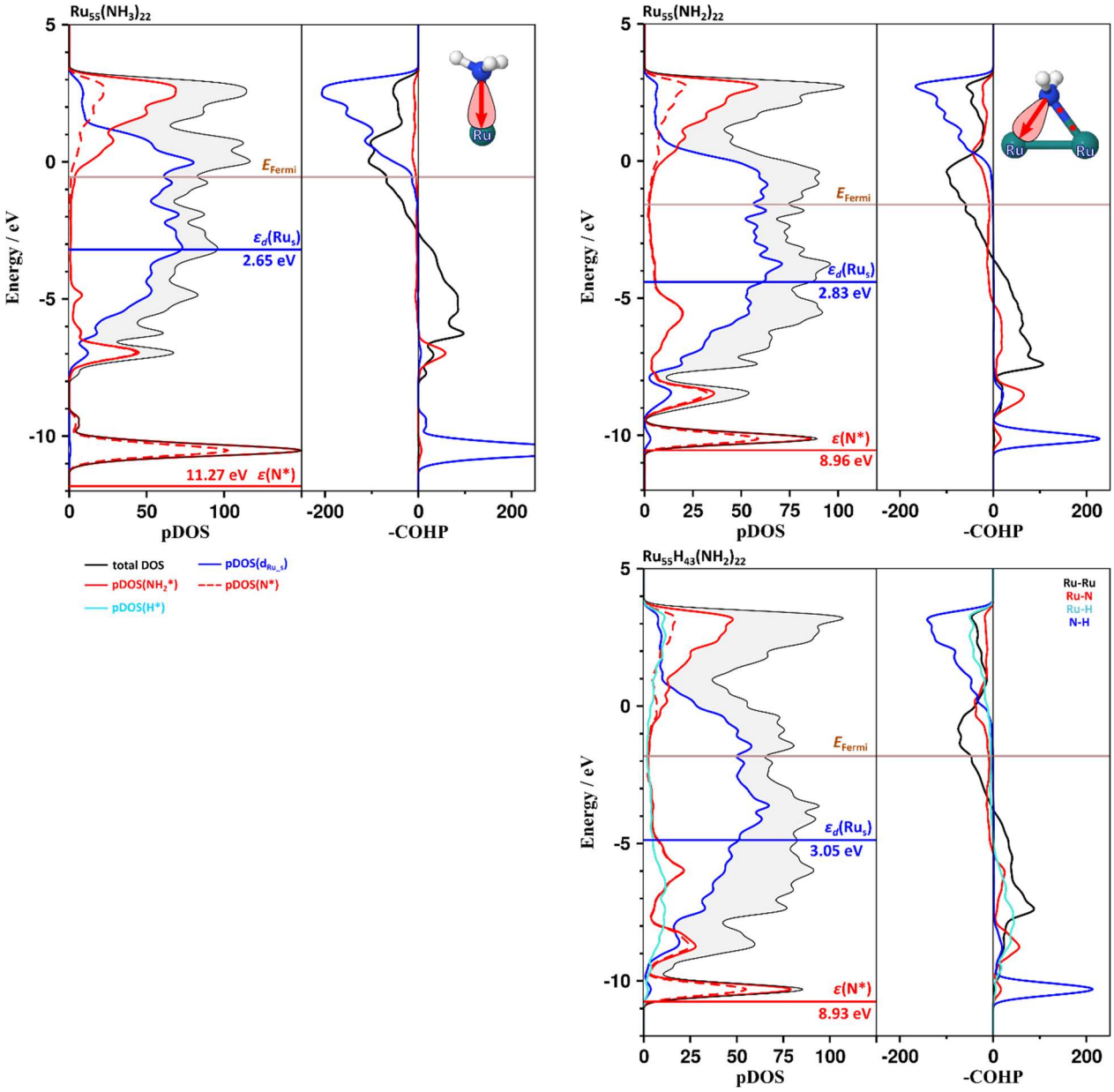

Figure S6. Density of states (DOS), selection of DOS projected on AOs (pDOS) and COHP profiles for $Ru_{55}(NH_3)_{22}$, $Ru_{55}(NH_2)_{22}$ and $Ru_{55}H_{43}(NH_2)_{22}$. The d-band center value, $\varepsilon_d(Ru_s)$, and the center of mass of the N* pDOS, $\varepsilon(N^*)$, are given relatively to the Fermi energy. A Lewis-like localized bonding scheme is also shown both for Ru-NH_3 and Ru_2-NH_2 fragments.

Let us first examine the DOS profile for $Ru_{55}(NH_2)_{22}$. First, no doubt about the metallic character of this nanocluster (blue profile). The d-projected DOS for surface Ru atoms, pDOS(d_{Ru_s}), relative to the Fermi energy, is in line with 7.2e/Ru occupation of this d band. $\varepsilon_d(Ru_s)$ lies 2.65 eV below the Fermi energy. It is very close to the value calculated for the bare Ru_{55} nanocluster, 2.57 eV (see also Table SIDFT1). This weak stabilization w.r.t. to Ru_{55} is in agreement with the weak σ-donor character of the NH_3 ligand. As already observed in previous

studies,[1] the pCOHP profile shows that the metal electronic states just below the Fermi energy are anti-bonding. The most stable metal states then acquire a metal-metal bonding character, and the overall cohesion of the metal surface is related to the excess of metal bonding states with respect to anti-bonding states. The simultaneous examination of the DOS and pCOHP profiles shows that the electronic states around -7 eV have components both on Ru and NH_3, resulting in a bonding Ru-N interaction (pCOHP profile, red curve). The bonding pattern is different for NH_2, with both a σ-donation and a covalent bonding. It can be seen both from the pDOS and pCOHP profiles and from electron charges reported in Table SIDFT1.

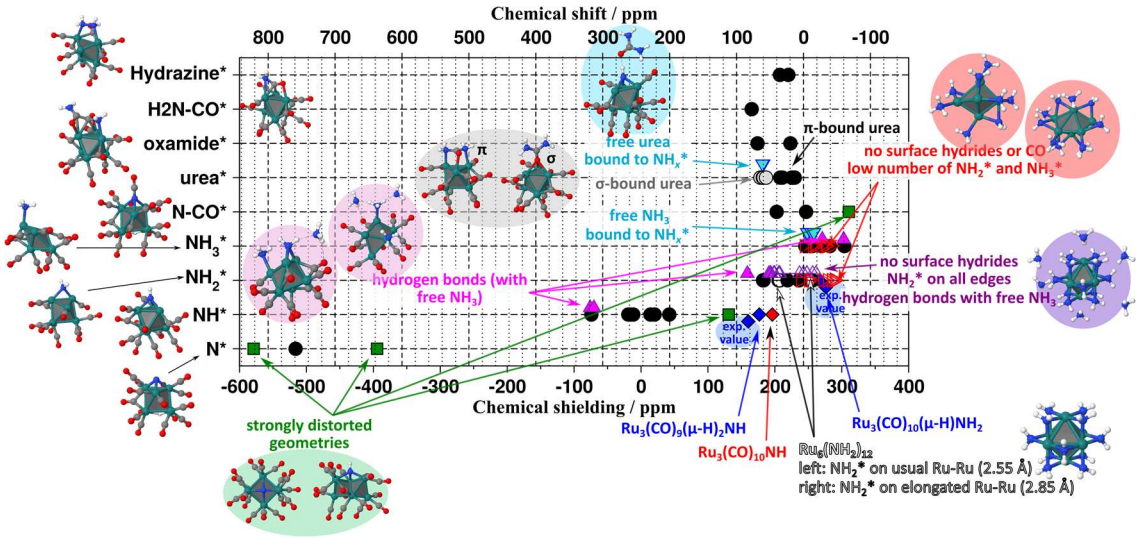

Figure S7. ^{15}N NMR chemical shieldings calculated in 46 [Ru_6] clusters at the DFT-PBE0 level of theory (* stands for "adsorbed"). Some geometries are also shown.

The chemical shielding is calculated by considering the simulated value of liquid ammonia at the same level of calculation: δ = σ(theoretical value for N in liquid ammonia) – σ(N of the sample); see computational details. These calculated chemical shieldings were used to define the resonance domains of Figure 5 of the article.

- Results are also given for nido [Ru_3] clusters with 48 (=14*n*+6) valence electrons (◆) and compared to experiments. [2] The agreement is very good.
- **η-NH_3** (on-top NH_3) systematically resonate at δ < 0, independent of the models, i.e. adsorbed on the [$Ru_6(CO)_n$] models (●), or making hydrogen bonds from the second sphere of coordination with surface species (▼), or adsorbed on undercoordinated [$Ru_6(NH_x)_n$] models (▷). Adsorbed NH_3 ligands are not significantly unshielded by hydrogen bonds with ammonia molecules in the gas phase (▲).
- The situation with **μ-NH_2** (edge-bridging NH_2) is more contrasted, i.e. the chemical shift is usually observed in the ~0 to 60 ppm domain (●), and again hydrogen bonds do not significantly unshield the NMR signal (▲). Negative chemical shifts are also found: δ(N) is observed both experimentally and theoretically at ~ -33 ppm for the very small $Ru_3(CO)_{10}(\mu\text{-H})NH_2$ cluster (◆); a strong shielding (δ ~ -11 ppm) is also calculated for NH_2 ligands adsorbed on significantly long Ru-Ru bonds on the $Ru_6(NH_2)_{12}$ cluster (○); it is even more strongly shielded for undercoordinated [$Ru_6(NH_x)_n$] models (▷), with δ ~ -20 to -40 ppm.
- In very small [Ru_3] clusters the ^{15}N NMR chemical shift of **μ$_3$-NH** (face-capping NH) is observed at ~ 50 – 80 ppm (●). When adsorbed on an atypical coordination site of one [$Ru_6(CO)_n$] model (■), N is found to resonate at ~ 105 ppm. Apart from these singular cases, μ_3-NH is expected to be observed in the ~ 200 to 300 pm domain.
- **μ$_3$-N** is strongly downfield shifted at ~ 750 ppm (●).

- NH_2 in σ-bound **urea** (see 3D representation on the Figure S8, urea is bound to the surface by the oxygen lone pairs) is found to resonate at the same value as free urea (●), *i.e.* ~ 60 ppm, whereas the π coordination involves a significant shielding by ~ 20 to 40 ppm (●). It turns out that π-coordinated urea could be observed in the same domain as μ-NH_2*, in line with the pyramidalization of the nitrogen atoms.
- **Hydrazine** has been considered as well. The simultaneous σ coordination of the two nitrogen lone pairs brings δ close to 30 ppm (●), similarly to π-coordinated urea and to "standard" edge-bridging (or μ) NH_2*.

Computational details.

DFT calculations of metal nanoclusters. Software: Vienna ab initio simulation package, VASP [3, 4]; spin polarized DFT; exchange-correlation potential approximated by the generalized gradient approach proposed by Perdew, Burke, and Ernzerhof (PBE) [5]; projector augmented waves (PAW) full-potential reconstruction [6, 7]; PAW data sets for Ru treating the (n-1)p, (n-1)d and ns states (*i.e.* 14 valence electrons); kinetic energy cutoff: 500 eV; Γ-centered calculations [8]; Gaussian smearing (σ) of 0.02 eV width, energies being therefore extrapolated for σ = 0.00 eV; geometry optimization threshold: residual forces on any direction less than 0.02 eV/Å; supercell size: 20×23×20 Å^3 (ensures a vacuum space of *ca*. 10 Å between periodic images of the nanoclusters).

Ru_{55} model. The model is a hcp spheroid. Its geometrical characteristics, as well as a H-coverage study were previously published in ref.[9]. It has also been used to study the adsorption properties of phenylpyridine [10] and of ethanoic acid [11] at the surface of hydrogenated RuNPs.

Adsorption energies.

$$E_{\text{ads}}(\text{H}) = \frac{1}{n}\left[E\left(n\text{H}^{*}\right) - E(\text{NP}) - \frac{n}{2}E(\text{H}_2)\right]$$

$$E_{\text{ads}}(\text{L}) = \frac{1}{n}\left[E\left(n\text{L}^{*}\right) - E(\text{NP}) - nE(\text{L})\right]$$

i.e. in the case of hydrides it is a dissociative adsorption energy.

COHP and DOS profiles. The LOBSTER package [12] which has been used in this work allows the calculation of Crystal Orbital Hamilton Population (COHP) curves projected onto an atomic Slater basis set (pCOHP), and also reliable atom-projected density of states (pDOS), both directly based on plane-wave wave-function calculated with the VASP package. The projection of the PAW wavefunction was achieved using the pbeVASPfit basis set. COHP is a partitioning of the band-structure energy in terms of orbital-pair contributions[13]. Some examples of its application to RuNPs can be found in Refs. [1, 9] and [10]

Charge calculations. A Mulliken population analysis (MPA) from VASP wavefunction was performed by integrating up to the Fermi energy with LOBSTER. The charge spilling, a criterion that assesses the quality of the projection, was systematically lower than 1.0%. A comparison of such MPA charges with other electronic density decomposition schemes (AIM-Bader, Natural Population Analyzis, CM5) can for example be found in ref. [14]

d-band center values (ε_d). They were calculated from the pDOS obtained with LOBSTER, see details in Ref.[1] The principle underlying this d-band center model[15] is that the binding energy of an adsorbate to a metal surface is largely dependent on the electronic structure of the surface itself. The closer ε_d to the Fermi energy (E_F), the stronger the bonding on the surface. A large ($E_F - \varepsilon_d$) involves weak adsorption energies.

NMR calculations. All DFT calculations on the [Ru_3] and [Ru_6] clusters were performed with Gaussian09.[16] Calculations were carried out at the DFT level of theory using the hybrid functional PBE0.[17] Geometry optimizations were achieved without any symmetry restriction. Calculations of vibrational frequencies were systematically done in order to characterize the nature of stationary points. Stuttgart effective core potential[18] and their associated basis set was used for Ruthenium, augmented by a set of polarization functions (ζ_f = 1.235). For the other elements (H, C, O, and P), Pople's polarized double-ζ basis set 6-31G(d,p)[19, 20] was used. The optimized structures were used for ^{15}N NMR calculations. Among the various theories available to compute chemical shielding tensors, the gauge including atomic orbital (GIAO) method was adopted for the numerous advantages it presents.[21-26] Calculating a theoretical chemical shift requires the knowledge of the chemical shielding of a reference, since it is explicitly calculated as $\delta = (\sigma_{ref} - \sigma)$, in ppm. We have shown in previous studies on ruthenium clusters that DFT-GIAO provides ^{1}H, ^{13}C in good agreement with experimental data and analysis.[27-30] The experimental reference chemical shift for ^{15}N corresponds to ammonia in its liquid phase. The theoretical ^{15}N chemical shift has been calculated using the same strategy as in Ref.[31], with $\sigma_{iso(ref)}$ = 242.8 ppm.[32] A previous study done on betaine adducts-protected RuNPs showed a good agreement between theoretical and experimental ^{15}N NMR chemical shifts. [31]

Ab initio thermodynamics. Let us consider a co-adsorption process of two species, L_1 and L_2, which is the starting point of the Langmuir–Hinshelwood mechanism in heterogeneous catalysis. It can be summarized as: MNP + n_1L_1 + n_2L_2 → n_1L_1* + n_2L_2*, (MNP = metal nanoparticle and * stands for "chemisorbed") and the Gibbs free energy for this reaction is calculated as:

$$\Delta G_{\text{ads}}(T, \text{L}_1, \text{L}_2) = [\Delta G° - n_1\mu(\text{L}_1) - n_2\mu(\text{L}_2)]/A$$

Where A is the surface area of the MNP, μ are chemical potentials and $\Delta G°$ is calculated after DFT energies and vibrational contributions to energies.

The free energy diagram of Figure 4 was calculated with our in-house *aithermo* software. Methodological details and examples of applications can be found in Refs. [1, 9, 11]. Yet, *aitermo* is made to study adsorption processes only, whereas for example accounting for $Ru_{55}(NH_2)_{22}$ would require to consider the reaction $Ru_{55}(NH_3)_{22}$ → $Ru_{55}(NH_2)_{22}$ + $11H_2$. This is why the stability diagram of Figure 4 is based on the calculation of $\Delta G_{\text{ads}}(T,p_{\text{H2}})$ for the following isomers only: $Ru_{55}(NH_3)_{22}$, $Ru_{55}H_{22}(NH_3)_{22}$, $Ru_{55}H_{44}(NH_3)_{22}$, $Ru_{55}H_{70}(NH_3)_{22}$, $Ru_{55}H_{33}(NH_3)_{11}(NH_2)_{11}$ and $Ru_{55}H_{55}(NH_3)_{11}(NH_2)_{11}$. It also explains the abrupt transition between the yellow and blue domains in Figure 4, that does not account for the preliminary conversion of NH_3 into NH_2. Such conversion is qualitatively introduced, given the NH_3 → NH_2 thermodynamic driving force calculated for low H coverage. The Ru-H vibrational contribution is accounted for, whereas Ru-N is neglected. The Ru-H vibrational contribution is accounted for, whereas Ru-N is neglected. The resulting stability diagram gives the most stable surface composition of the samples in equilibrium under a given pressure p_{H2} and temperature T. Mind that without other chemisorbed ligands, 1.6 H/Ru_{surface} was found to be the equilibrium composition under standard temperature and pressure conditions. It turned out to be in agreement with experimental quantitative analysis done on RuNPs stabilized with PVP. [9] Such model incorporates an elongated, undissociated H_2 on an apex, in line with the weaker back donation from the metal to the σ*(H_2) MO for such highly saturated RuNPs. On lowering surface coverage, dihydrogen molecules dissociate on the surface.

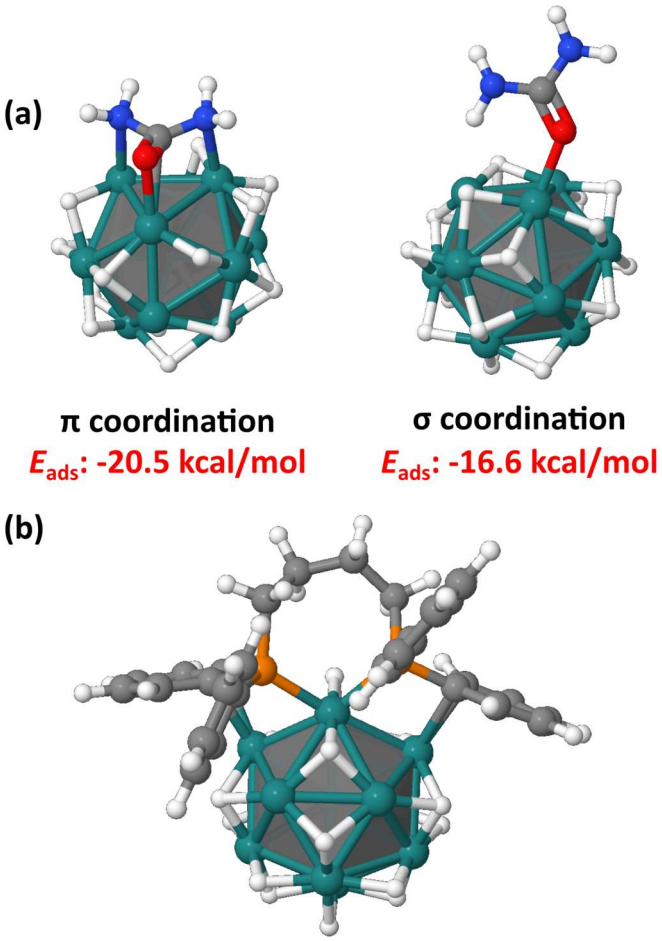

Figure S8: Adsorption of (a) urea or (b) dppb on an hydrogenated Ru13 model cluster.

1. L. Cusinato, I. del Rosal and R. Poteau, *Dalton T.*, 2017, **46**, 378-395.
2. J. A. Smieja, R. E. Stevens, D. E. Fjare and W. L. Gladfelter, *Inorg. Chem.*, 1985, **24**, 3206-3213.
3. G. Kresse and J. Furthmüller, *Phys. Rev. B*, 1996, **54**, 11169-11186.
4. G. Kresse and J. Furthmüller, *Computational Materials Science*, 1996, **6**, 15-50.
5. J. P. Perdew, K. Burke and M. Ernzerhof, *Phys. Rev. Lett.*, 1996, **77**, 3865-3868.
6. P. E. Blöchl, *Phys. Rev. B*, 1994, **50**, 17953-17979.
7. G. Kresse and D. Joubert, *Phys. Rev. B*, 1999, **59**, 1758-1775.
8. H. J. Monkhorst and J. D. Pack, *Phys. Rev. B*, 1976, **13**, 5188-5192.
9. L. Cusinato, L. M. Martínez-Prieto, B. Chaudret, I. del Rosal and R. Poteau, *Nanoscale*, 2016, **8**, 10974-10992.
10. J. Creus, S. Drouet, S. Suriñach, P. Lecante, V. Collière, R. Poteau, K. Philippot, J. García-Antón and X. Sala, *ACS Catalysis*, 2018, **8**, 11094-11102.

11. R. González-Gómez, L. Cusinato, C. Bijani, Y. Coppel, P. Lecante, C. Amiens, I. del Rosal, K. Philippot and R. Poteau, *Nanoscale*, 2019, **11**, 9392-9409.
12. S. Maintz, V. L. Deringer, A. L. Tchougreeff and R. Dronskowski, *J. Comput. Chem.*, 2016, **37**, 1030-1035.
13. R. Dronskowski and P. E. Bloechl, *J. Phys. Chem.*, 1993, **97**, 8617-8624.
14. I. C. Gerber and R. Poteau, *Theoretical Chemistry Accounts*, 2018, **137**.
15. B. Hammer and J. K. Norskov, *Surf. Sci.*, 1995, **343**, 211-220.
16. M. J. T. Frisch, G. W.; Schlegel, H. B.; Scuseria, G. E.; Robb, M. A.; Cheesman, J. R.; Scalmani, G.; Barone, V.; Mennucci, B.; Petersson, G. A.; Nakatsuji, H.; Caricato, M.; Li, X.; Hratchian, H. P.; Izmaylov, A. F.; Bloino, J.; Zheng, G.; Sonnenberg, J. L.; Hada, M.; Ehara, M.; Toyota, K.; Fukuda, R.; Hasegawa, J.; Ishida, M.; Nakajima, T.; Honda, Y.; Kitao, O.; Nakai, H.; Vreven, T.; Montgomery, J. A., Jr.; Peralta, J. E.; Ogliaro, F.; Bearpark, M.; Heyd, J. J.; Brothers, E.; Kudin, K. N.; Staroverov, V. N.; Kobayashi, R.; Normand, J.; Raghavachari, K.; A., R.; Burant, J. C.; Iyengar, S. S.; Tomasi, J.; Cossi, M.; Rega, N.; Millam, M. J.; Klene, M.; Knox, J. E.; Cross, J. B.; Bakken, V.; Adamo, C.; Jaramillo, J.; Gomperts, R.; Stratmann, R. E.; Yazyev, O.; Austin, A. J.; Cammi, R.; Pomelli, C.; Ochterski, J. W.; Martin, R. L.; Morokuma, K.; Zakrzewski, V. G.; Voth, G. A.; Salvador, P.; Dannenberg, J. J.; Dapprich, S.; Daniels, A. D.; Farkas, O.; Foresman, J. B.; Ortiz, J. V.; Cioslowski, J.; Fox, D. J., *Gaussian 09, Revision D.01*, Wallingford CT, 2009.
17. C. Adamo and V. Barone, *J. Chem. Phys.*, 1999, **110**, 6158-6170.
18. A. Bergner, M. Dolg, W. Kuchle, H. Stoll and H. Preuss, *Mol. Phys.*, 1993, **80**, 1431-1441.
19. P. C. Hariharan and J. A. Pople, *Theor. Chim. Acta*, 1973, **28**, 213-222.
20. W. J. Hehre, R. Ditchfield and J. A. Pople, *J. Chem. Phys.*, 1972, **56**, 2257-2261.
21. R. Ditchfield, *Mol. Phys.*, 1974, **27**, 789-807.
22. K. Wolinski and A. J. Sadlej, *Mol. Phys.*, 1980, **41**, 1419-1430.
23. P. C. Junk and J. W. Steed, *J. Organomet. Chem.*, 1999, **587**, 191-194.
24. F. London, *J. Phys. Radium*, 1937, **8**, 397-409
25. R. McWeeny, *Phys. Rev.*, 1962, **126**, 1028-1034.
26. K. Wolinski, J. F. Hinton and P. Pulay, *J. Am. Chem. Soc.*, 1990, **112**, 8251-8260.
27. I. del Rosal, T. Gutmann, L. Maron, F. Jolibois, B. Chaudret, B. Walaszek, H.-H. Limbach, R. Poteau and G. Buntkowsky, *Phys. Chem. Chem. Phys.*, 2009, **11**, 5657-5663.
28. I. del Rosal, T. Gutmann, B. Walaszek, I. C. Gerber, B. Chaudret, H.-H. Limbach, G. Buntkowsky and R. Poteau, *Phys. Chem. Chem. Phys.*, 2011, **13**, 20199-20207.
29. I. del Rosal, F. Jolibois, L. Maron, K. Philippot, B. Chaudret and R. Poteau, *Dalton T.*, 2009, DOI: 10.1039/b817055j, 2142-2156.
30. I. del Rosal, L. Maron, R. Poteau and F. Jolibois, *Dalton T.*, 2008, DOI: 10.1039/b802190b, 3959-3970.
31. L. M. Martínez-Prieto, I. Cano, A. Márquez, E. A. Baquero, S. Tricard, L. Cusinato, I. del Rosal, R. Poteau, Y. Coppel, K. Philippot, B. Chaudret, J. Cámpora and P. W. N. M. van Leeuwen, *Chem. Sci.*, 2017, **8**, 2931-2941.
32. I. C. Gerber and F. Jolibois, *Phys. Chem. Chem. Phys.*, 2015, **17**, 12222-12227.